Title
NEUTRON TRANSFER REACTIONS WITH VERY HEAVY IONS

Author
Macchiavelli, A.O.

Publication Date
1984-03-01

Lawrence Berkeley Laboratory
UNIVERSITY OF CALIFORNIA

Submitted to Nuclear Physics

NEUTRON TRANSFER REACTIONS WITH VERY HEAVY IONS

A.O. Macchiavelli, M.A. Deleplanque, R.M. Diamond,
F.S. Stephens, E.L. Dines, and J.E. Draper

March 1984

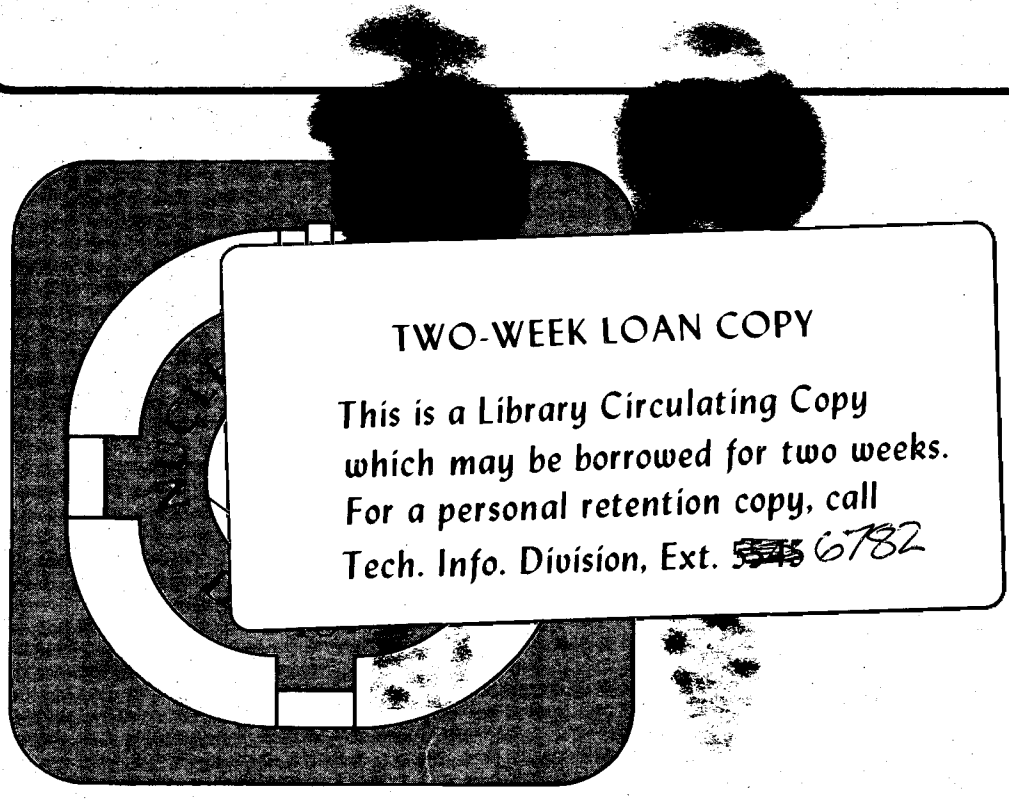

Prepared for the U.S. Department of Energy under Contract DE-AC03-76SF00098

DISCLAIMER

LBL-17647

Neutron transfer reactions with very heavy ions

A. O. Macchiavelli,[+] M. A. Deleplanque, R. M. Diamond,
F. S. Stephens, E. L. Dines,[++] and J. E. Draper[++]

Nuclear Science Division
Lawrence Berkeley Laboratory
University of California
Berkeley, California 94720

Abstract: We have studied neutron transfer reactions induced by ^{132}Xe on three rare-earth targets at $E/V_c \sim 1.1$. By using particle-particle-γ coincidence techniques we were able to identify final products and states populated in the one- and two-neutron reactions.

The dependence of the transfer probabilities on the distance of closest approach is discussed in terms of effective penetration factors. The results seem to indicate the importance in 2n-transfer of intermediate states with ≈6 MeV of excitation energy. The effect of excitation energy on the enhancement of the two-neutron transfer is discussed. A qualitative interpretation of the spin dependence of the one-neutron γ-ray yields in terms of the spatial localization of the wave functions involved is given.

NUCLEAR REACTIONS: ^{154}Sm, ^{176}Yb, ^{171}Yb + ^{132}Xe, $E/V_c \sim 1.1$; particle-particle-γ coincidence technique; measured γ-ray yields; deduced one- and two-neutron transfer probabilities.

This work was supported by the Director, Office of Energy Research, Division of Nuclear Physics of the Office of High Energy and Nuclear Physics of the U.S. Department of Energy under Contract DE-AC03-76SF00098.

[+]Permanent Address: Comisión Nacional de Energía Atómica, Buenos Aires, Argentina.

[++]Permanent Address: Department of Physics, University of California, Davis, CA 95616

I. Introduction

Transfer reaction studies with light ions (e.g. (t,p), (p,d), etc.) have provided very useful information on nuclear structure; both single-particle aspects and residual interactions (such as pairing) have been studied by one- and two-nucleon transfer reactions [1]. Later, transfer reactions with light heavy ions have been used to study nuclei near closed shells [2], and still more recently, selective population of high-j orbitals in deformed Er nuclei was observed using transfer reactions induced by ^{12}C and ^{16}O, due to a favorable angular momentum mismatch between the entrance and exit channels [3].

In this paper, we want to consider transfer reactions with very heavy ions ($A > 40$). There are a number of reasons why these reactions are an interesting and attractive tool for nuclear physics [4]. We would like to summarize some of the ones we consider important:

i) They can provide information similar to that obtained with light-ion reactions, but with the unique features associated with very heavy ions, namely, the interplay between single-particle aspects, particle-particle correlations and collective excitations.

ii) They can populate states that cannot be produced with other reactions, for example, high-spin states in nuclei that cannot be reached with conventional (HI, xn) reactions, or with Coulomb excitation.

iii) The small amount of mass, angular momentum and energy transferred, i.e., $\Delta M/M$, $\Delta L/L$ and $\Delta E/E \ll 1$, which together with the large Sommerfeld parameter, $\eta \gg 1$, give the possibility of defining a localized classical trajectory for the reaction.

In the last few years several studies have been devoted to transfer reactions with very heavy ions. Proton transfer reactions in the systems ^{86}Kr on ^{88}Sr, ^{90}Zr, and ^{92}Mo near the Coulomb barrier were studied by H. Siekmann et al. [5]) by detecting the reaction products in a wide-angle ionization chamber. G. Himmele et al. [6]) reported results on neutron transfer in $^{184}W + ^{238}U$, also near the Coulomb barrier. They have measured conversion electrons in coincidence with the backscattered projectile to identify the products. In both studies an enhancement of the cross-section for 2-nucleon transfer was found, and effective exponential form factors were obtained for the reactions considered. W. von Oertzen et al. [7]) have discussed pairing effects in quasi-elastic neutron transfer in the reaction $^{120}Sn + ^{112}Sn$ at energies below the Coulomb barrier.

In the present work we have extended particle-γ coincidence methods to very heavy-ion transfer reactions; the techniques have been used previously in Coulomb-nuclear interference studies [8]). We used a Xe beam on rare-earth targets to explore some of the previously discussed aspects of these kinds of reactions. The results, though still qualitative, provide an idea of the information one may get from such a technique in this yet poorly explored field.

II. Experimental Method and Results

In Table I, we have summarized the reactions studied, and have included some parameters related to their dynamics. For comparison, the same parameters are listed for ^{16}O and d projectiles. Note the strong collective excitation (indicated by I_{max}) induced by Xe projectile and the very large value of η. ^{16}O does not produce as much collective excitation, and a classical trajectory is impossible to define with deuterons ($\eta \simeq 1$).

The Xe beam was provided by the LBL SuperHILAC and the targets were self-supporting rare-earth metal foils of $\simeq 0.5$ mg/cm^2. The experimental arrangement consisted of two large-solid-angle ($\simeq 20^\circ \times 15^\circ$) position-sensitive gas avalanche detectors (PSAD) to detect the coincident projectile- and target-like products, while two Ge(Li) counters placed at 180° to the PSAD's were used to observe the γ-rays emitted in the reaction. A schematic layout is shown in fig. 1. The PSAD to the right of the beam direction was centered at the grazing angle for a Coulomb trajectory:

$$\theta_{gra,cm} = 2 \arctan \left(X/\sqrt{1 - X^2}\right)$$

$$X = 1/(2E_{cm}/V_c - 1) \qquad \text{(II-1)}$$

E_{cm} being the center of mass energy and V_c the Coulomb barrier. The position of the other detector was determined by classical kinematics. A particle-particle-γ coincidence was required as a master gate. The x,y positions in both PSAD's, the Ge(Li) signals, the TAC between the PSAD's, the particle-γ TAC's and the scaled-down particle-particle coincidences were recorded event-by-event on magnetic tapes. Standard ^{152}Eu and ^{60}Co

sources were used to get energy and efficiency calibrations for the Ge(Li) detectors. A ^{252}Cf source was used to calibrate the x,y positions in the PSAD's.

The sorting of the data was done off-line and proceeded through the following steps:

A) Two 2-D spectra were generated from the x positions in the PSAD's and the TAC signal between them. The different timing characteristics of the distant and close collisions allowed a clear separation of them, and 2-D gates were set selecting those events associated with one or the other type of collision. A typical 2-D spectrum is shown in fig. 2.

B) Five cuts in the x position of the right PSAD defined five different scattering angles. This procedure was also used to correct for the Doppler broadening of the coincident γ-lines due to the recoil of the target-like ion into vacuum.

C) A prompt particle-γ TAC signal was required before generating the Ge(Li) spectra.

D) For each angle the scaled-down singles were also obtained to normalize the spectra.

This technique therefore combines intermediate resolution for the fragments to define the "classical trajectory" of the collision and the high resolution possible with γ-rays to identify products and states populated in the reaction process. Fig. 3 shows Ge(Li) spectra in coincidence with distant- and close-collision events for the ^{154}Sm target. The good separation achieved by the 2-D gates can be noted. In figs. 4 and 5 we present the spectra for the ^{176}Yb, ^{171}Yb cases; only spectra associated with close-collision events are shown. It is important to note that the presence

of impurities in the target (e.g., ^{152}Sm, etc.) will be reflected immediately in the "distant collisions" γ-spectra, while light contaminants (e.g., ^{16}O, etc.) will not trigger the coincident particle detectors due to different kinematics.

III. Analysis and Discussion

III.1 Total probabilities

From the yield of γ rays de-exciting a level of spin I_o, corrected by the efficiency of the γ detector, we get the number of particle-particle-γ coincidences $N_{p-p-\gamma}$ for a given scattering angle θ in the center of mass. The number of particle-particle coincidences N_{p-p} is given by the scaled-down singles. The ratio $N_{p-p-\gamma}/N_{p-p}$ defines the total probability of populating that particular-state directly or indirectly, i.e.,

$$\frac{N_{p-p-\gamma}(\theta, I_o)}{N_{p-p}(\theta)} = \sum_{I \geq I_o} P_I(\theta) \qquad \text{(III-1)}$$

The right side of eq. (III-1) is strictly true if we have a monotonic relation between energy and spin, a condition which is fulfilled by the rotational bands in the nuclei studied.

In figs. 6 and 7 we summarize the results for the γ-ray yields integrated over the solid angle of the particle detector, as a function of spin. For the inelastic reactions (i.e., Coulomb + Nuclear scattering interactions) the yield saturates for $I_o \leq 6^+$ and a strong population of the ground and 2^+ states can be ruled out. Then $\sum_{I \geq 4} P_I$ will give us the total probability P_o of producing an inelastic collision. Similarly we can get the total probability $P_{\Delta N}$ for the transfer channels. Table II summarizes the values found.

Since the values for P_o are around 30%, we have to conclude that we are in a regime where multiparticle transfer and deep-inelastic reactions are important. To understand this effect we can attribute it to the imaginary

potential W(r). In a simple approximation one considers a damping factor of the form:

$$d_{fac} = \exp(\frac{1}{\hbar} \int_{trajectory} W(r(t))dt) \qquad \text{(III-2)}$$

and the probability to remove the collision from the inelastic channel will be $\approx d_{fac}^2$. Expanding around the distance of closest approach r_o:

$$d_{fac} = \exp(\frac{4}{3\hbar} W(r_o)\tau)$$

$$\tau = [2\mu\, W(r_o)/(\frac{\partial W}{\partial r}(r_o)\frac{\partial V}{\partial r}(r_o))]^{1/2} \qquad \text{(III-3)}$$

where μ is the reduced mass of the system and V the real part of the potential. With the parameters of ref [4]) one gets $d_{fac}^2 \approx 0.9 - 0.5$ depending on the distance of closest approach considered for the different reactions. The large absorption probabilities observed in ref [5]) were associated with deep-inelastic collisions, and recently large cross sections for nucleon transfer (quasi-elastic + deep-inelastic), around 70% of σ_R, have been observed [9]) for ^{58}Ni on ^{208}Pb at $E/V_c \sim 1.25$. These deep-inelastic products will fire our PSAD's but the γ-rays associated with them are likely to form a continuum spectrum due to the low population of individual channels. Therefore, we think that the discrete γ-lines we have observed are related to quasi-elastic events (Q-windows < 10 MeV).

III.2 Effective penetration factors and enhancement

As pointed out previously, the scattering angle of the projectile defines a classical trajectory. If this is not very different from a Coulomb trajectory, one is able to define a distance of closest approach through

$$D(\theta) = \eta/k(1 + 1/\sin\theta/2) \qquad \text{(III-4)}$$

k being the wave number. The transfer probabilities as a function of D(θ) are presented in fig. 8 for the different reactions. All the cases show an exponential behavior, i.e.,

$$P_{\Delta N}(D(\theta)) \alpha \exp(-K\ D(\theta)) \qquad \text{(III-5)}$$

For reactions below the Coulomb barrier the transfer of nucleons is usually described by a barrier penetration model [10], and the parameter K is given by $2\sqrt{2mB}$ where B is the average ground-state binding energy of the transferred particle. Above the Coulomb barrier, we can interpret K in (III-5) as an effective penetration factor $K_{eff} = 2\sqrt{2mB}_{eff}$; table III shows the values of K_{eff} obtained for the cases in fig. 8.

The values for one-neutron transfer are in reasonable agreement with the values calculated using the appropriate ground-state binding energies. On the other hand, it is expected in either sequential or direct transfer of two neutrons that $K_{2n} \simeq 2\ K_{1n}$. This fact is clearly not observed for K_{eff} in this experiment nor in the results of ref [2,5,6].

The values of the effective binding energies found seem to indicate that intermediate states with higher excitation energies may be important for the

transfer of two neutrons at energies above the Coulomb barrier. We can estimate an average excitation energy around 6 MeV in order to reproduce the effective binding energy, B_{eff}, in table III.

As in refs [5,6]), we can define an enhancement factor that relates the observed probabilities for 2n transfer to that of an uncorrelated pair. At any distance D(θ),

$$EF(D) = \frac{P_{2n}(D)}{P_{1n}^2(D)} \qquad \text{(III-6)}$$

After applying a small correction due to the effects of the kinematics of the reaction [11,12]) values of EF ≅ 5 - 30 are found. An interesting interpretation of this enhancement factor is to relate it to the pairing interaction. One expects pairing to enhance 2n-transfers both in a single- (true-pair) and two-step (sequential) process [1,13]). The authors of ref [7]) have shown that by lowering the bombarding energy below the Coulomb barrier, penetration factors are well reproduced by the average ground-state binding energies.* Then a proper discussion of pairing effects is possible. However, as discussed previously, above the Coulomb barrier 2n-transfer probably proceeds via states of higher excitation energy. Due to the smaller effective barrier the probability for 2n-transfer is in this case larger than that expected for a cold transfer. For example, let us consider a simple schematic mechanism. We retain a barrier penetration description of the transfer

---

*It should be mentioned that some problems in the normalization of their data still remain. This results from the large probabilities observed for transfer, that should be included them in the total probability.

process (this may not be justified) and assume two paths contributing to the total possibilities: one cold (P_i) and one excited (P_i^*). Then

$$P_{1n,T} \cong P_{1n} + P_{exc}\ P_{1n}^* = P_{1n} + \tilde{P}$$

$$P_{2n,T} \cong P_{1n}^2 + 2P_{exc}P_{1n}P_{1n}^* + P_{exc}P_{1n}^{*2} = P_{1n}^2 + 2P_{1n}\tilde{P} + P_{1n}^*\tilde{P} \qquad \text{(III-7)}$$

where P_{exc} represents the probability of having the nucleus excited. While the excitation energy ($\tilde{P}$ terms) has a small effect on $P_{1n,T}$, it is the main contribution to $P_{2n,T}$ (see fig. 9). In this way we can extract from the data a value for EF around 2.5. This result shows that under the assumptions leading to eq. III-7, the "apparent" large EF could be explained without resort to the pairing correlations. To summarize, it appears that although we cannot rule out an enhancement due to the pairing interaction, the effect of excitation energy should not be ignored when discussing enhancement factors.

III.3 Spin dependence of the probabilities

Finally we turn our attention back to fig. 6 and 7, and discuss the spin dependence of the probabilities. We start with the inelastic channels. Both ^{154}Sm and ^{176}Yb have the same pattern. Actually, this result is expected since both nuclei have the similar quadrupole moments $Q_o^{(2)}$ (see values of I_{max} in table I). Moreover, since the classical trajectories, which determine the distance of closest approach, are similar, the effects of the nuclear potential on the spin population are also expected to be similar. ^{171}Yb also presents the same yield pattern for the same reason, as it has a low-spin ground state (1/2).

In order to get a more quantitative description of the effect of the nuclear potential V_N, we have considered the case of a sudden backward collision between ^{132}Xe and ^{154}Sm. To calculate the expected γ-ray yield we have used the classical limit S-matrix method [14]) for the cases $V_N = 0$ and $V_N = 120$ [4]). The laboratory energy was fixed to match the distance of closest approach in the actual collision. The results are compared in fig. 10. Although we should not take too seriously the good agreement between the experimental points and the case $V_N = 120$ MeV, the presence of the attractive nuclear potential clearly manifests itself by depressing the population of the high spins.

We consider now the 2n-transfer reactions in ^{154}Sm and ^{176}Yb. Here it is difficult to extract unambiguously the initial spin population because the γ-lines could reflect both "cold" processes and the decay of excited states into the yrast band. The experimental results show that the shape of the populations follow closely that of the inelastic channels. This effect may be due to a smearing out of the initial population as the nucleus decays towards the yrast states.

We are more confident that in the 1n-transfer the γ-ray yields reflect the initial spin population. To understand the observed pattern for the transfer of 1n to form the $i_{13/2}$ band in ^{153}Sm we refer to fig. 11. If, at the moment of transfer, the even-even target has been excited to spin R then one expects to transfer to $I \sim I_x = R + j_x$. In the second half of the collision it will gain approximately another R units of spin. Thus the population for γ-decay will be centered around $R + j_x + R$. From fig. 7 this spin is $\cong 21/2$. Now we need to estimate j_x for the $i_{13/2}$ band states. Using the wave function obtained in ref [15]) we calculate $j_x = 5.5$ for the

$I = 17/2$ state. This tells us that transfer to give the $i_{13/2}$ band in ^{153}Sm is on average associated with collisions that transfer small amounts of collective angular momentum i.e. $R \simeq 2$. This effect may be related to spatial localization of the Nilsson levels involved. The particle in those states will be mainly concentrated near the poles of the nucleus, thus favoring polar collisions that transfer small amounts of collective angular momentum to the target. A similar argument holds for the transfer of 1n to form the ground-state band in ^{170}Yb. The relevant Nilsson state in this case is 1/2[521] ($p_{3/2}$ parentage). Since this configuration is expected to have no strong localization in space and since j_x is small, the γ-ray yields should follow those of the inelastic channel as is observed experimentally.

IV. Conclusions

In summary we have explored transfer reactions between very heavy ions by studying reactions of ^{132}Xe on rare earth targets using particle-particle-γ coincidence techniques. One- and two-neutron transfers were clearly seen in the γ-ray spectra. The effective form factors (eq. III-5) found suggest the importance of intermediate states of ~6 MeV excitation energy for the transfer of two neutrons. This observation casts some doubts on the interpretation of the "apparent" enhancement factor as arising from the pairing interaction [5,6]. In the framework of a simple mechanism we could show that without pairing the observed probabilities could be approximately explained.

We have discussed qualitatively the spin population patterns. The "inelastic" γ-rays reveal the effect of the nuclear potential and the results for one-neutron transfer could be explained considering the spatial localization of the single-particle states involved. On the other hand, it is more difficult to interpret the two-neutron transfer results because they may not reflect solely the initial population.

We believe these kinds of reactions may become a useful tool for nuclear structure studies at high spins. To investigate further pairing effects in the 2n-transfer and spatial localization signatures we are currently planning experiments that will use Compton-suppressed Ge arrays [16] in combination with recently developed particle detectors [17]. In such experiments the statistics will be improved by a large factor, opening the possibility of a more quantitative analysis.

The authors would like to thank D. Habs for his participation in the early stages of this work, particularly in the design of the PSAD's and the scattering chamber. Discussions with T. Døssing and J. O. Rasmussen are greatly appreciated.

This work was supported by the Director, Office of Energy Research, Division of Nuclear Physics of the Office of High Energy and Nuclear Physics of the U.S. Department of Energy under Contract DE-AC03-76SF00098.

References

(1) B. Elbek and P. Tjøm, Adv. Nucl. Phys. 3 (1969) 259
R. A. Broglia, O. Hansen and C. Riedel, Adv. Nucl. Phys. 6 (1973) 287 and references therein.

(2) F. D. Becchetti, Proceedings of Heavy-Ions Summer Study, Oak Ridge, TN, 1972, p. 163
S. Kahana and A. J. Baltz, Adv. Nucl. Phys. 9 (1977) 1 and references therein.

(3) P. D. Bond, J.Barrette, C. Baktash, C. E. Thorn and A. J. Kreiner, Phys. Rev. Lett. 46 (1981) 1565

(4) M. W. Guidry, T. L. Nichols, R. E. Neese, J. O. Rasmussen, L. F. Oliveira and R. Donangelo, Nucl. Phys. A361 (1981) 275
C. H. Dasso, T. Døssing, S. Landowne, R. A. Broglia and A. Winther, Nucl. Phys. A389 (1982) 191

(5) H. Siekmann et al., Z. Phys. A307 (1982) 113

(6) G. Himmele, H. Backe, P. A. Butler, D. Habs, V. Metag, H. J. Specht and J. B. Wilhelmy, Nucl. Phys. A404 (1983) 401

(7) W. von Oertzen, B. Gebauer, A. Gamp, H. G. Bohlen, F. Busch and D. Schull, Z. Phys. A313 (1983) 189

(8) M. Guidry et al., Phys. Rev. Lett. 40 (1978) 1016

(9) K. D. Rehm, D. G. Kovar, W. Kutschera, M. Paul, G. Stephans and J. L. Yntema, Phys. Rev. Lett. 51 (1983) 1426

(10) G. Breit and M. E. Ebel, Phys. Rev. 103 (1956) 679

(11) K. Alder, R. Morf, M. Pauli and D. Trautmann, Nucl. Phys. A19 (1972) 399

(12) R. A. Broglia, G. Pollarollo, A. Winther, Nucl. Phys. A361 (1981) 307

(13) U. Gotz, M. Ichimura, R. A. Broglia, A. Winther, Phys. Rep. 16C (1975) 115
H. Weiss, Phys. Rev. 19C (1979) 834
W. von Oertzen, R. E. Brown, E. R. Flynn, J. C. Peng and J.W. Sunier, Z. Phys. A313 (1983) 371

(14) R. Donangelo, PhD Thesis (1977) University of California and references therein.

(15) J. Rekstad, M. Guttormsem, T. Engeland, G. Løvhøiden, O. Straume, J. Lien and C. E. Ellegaard, Nucl. Phys. A320 (1979) 239

(16) R. M. Diamond and F. S. Stephens, proposal for a High-Resolution Ball, Sept. 1981, unpublished

(17) D. Cline, private communication, 1983

Table Captions

Table I Some properties of the reactions studied. The formulas are given which were used to calculate the Coulomb barrier (V_c), the interaction radius (R), the Sommerfeld parameter (η), the grazing angular momentum (L_g) and the maximum collective spin transferred in a sudden backward collision (I_{max}). For comparison, the same properties are considered for ^{16}O and deuterons as projectiles.

Table II Summary of the probabilities observed for the different channels.

Table III Effective penetration factors, K_{eff}, and the calculated values, K, using ground-state binding energies.

TABLE I

Reaction	E_{lab} (MEV)	E_{cm}/V_c	R (fm)	n	L_g	I_{max}
$^{132}Xe + ^{154}Sm$	690	1.09	14.44	232	146	≈26
$^{132}Xe + ^{176}Yb$	720	1.08	14.73	254	152	
$^{132}Xe + ^{171}Yb$	720	1.08	14.66	254	151	
$^{16}O + ^{154}Sm$	78.5	1.09	11.15	35	22	8
$d + ^{154}Sm$	9.86	1.09	10.	3.8	3	0

Where:

$$V_c = 1.44\ Z_p Z_t / R$$

$$R = 1.16\ (A_p^{1/3} + A_t^{1/3} + 2)$$

$$n = Z_p Z_t e^2/\hbar V_o = 0.157\ Z_p Z_t \sqrt{A_p/E_{LAB}}$$

$$L_g = 0.219\ R \sqrt{\mu(E_{cm} - V_c)}$$

$$I_{max} = 2n\ Q_o^{(2)}(E_{cm}/V_c)^2/R^2$$

TABLE II

Reaction	ΔN	Q_{gg}(MeV)	$P_{\Delta N}$(%)
$^{132}Xe + ^{154}Sm$	0	0	22±1
	+1 n	-1.52	7±1
	+2 n	1.14	3.5±0.5
	-2 n	-2.49	0.7±0.3
$^{132}Xe + ^{176}Yb$	0	0	21±1
	+1 n	-0.43	3.8±0.6
	+2 n	2.29	2.0±0.3
$^{132}Xe + ^{171}Yb$	0	0	35±2
	+1 n	-0.17	3.0±0.5
	-1 n	-0.92	≈3±1 [a)]

a) Larger uncertainty due to ^{172}Yb impurity in the target.

TABLE III

Reaction	ΔN	K_{eff} (fm^{-1})	$K = 2\sqrt{2MB}$	B_{eff} (MeV)	B
$^{132}Xe + ^{154}Sm$	+1 n	1.1 ± 0.2	1.24	6.	8.
	+2 n	1.1 ± 0.2	2.30	3.1	13.8
$^{132}Xe + ^{176}Yb$	+1 n	1.0 ± 0.2	1.15	4.7	6.9
	+2 n	1.0 ± 0.2	2.21	2.4	12.7
$^{132}Xe + ^{171}Yb$	+1 n	1.0 ± 0.2	1.13	4.7	6.6

Figure Captions

Fig. 1 Schematic layout of the experimental arrangement. Distant- and close-collision events are represented by the dotted- and dashed-lines, respectively (thick symbols correspond to target-like fragments). On the insert is sketched a γ line from the target as seen by the Ge(Li) to the right of the beam direction.

Fig. 2 A typical 2-D spectrum used to select distant- and close-collision events. ΔT is the time difference between the two PSAD's.

Fig. 3 Gamma ray spectra seen by Ge(Li)-R for the ^{154}Sm runs.
Bottom: in coincidence with distant-collision events
Top: in coincidence with close-collision events, the transfer lines are now clearly seen.

Fig. 4 Gamma ray spectra in coincidence with close-collision events for the ^{176}Yb run; again transfer lines are identified.

Fig. 5 Same as fig. 4 but for the ^{171}Yb case.

Fig. 6 Gamma-ray yields as a function of spin for the inelastic channels. Representative errors are shown for one nucleus. Lines shown are to guide the eye.

Fig. 7 Same as fig. 6 but for the transfer channels.

Fig. 8 Probabilities for transferring one and two neutrons as a function of the distance between the two nuclei. The effective penetration factors are extracted from the slopes of the lines shown.

Fig. 9 Contributions from cold (P_i) and excited (P_i^*) transfers to the total probability ($P_{i,T}$). An EF ~ 2.5 is needed to reproduce the experimental 2n-points.

Fig. 10 Comparison of the experimental inelastic γ-ray yields for the $^{132}Xe + ^{154}Sm$ case with a theoretical calculation based on the CLSM method of ref [14]. Two cases are considered $V_N = 0$ (----) and $V_N = 120$ MeV (——).

Fig. 11 Expected configuration of collective ($\vec{R}$) and single particle ($\vec{j}$) angular momenta to form the $i_{13/2}$ band in ^{153}Sm.

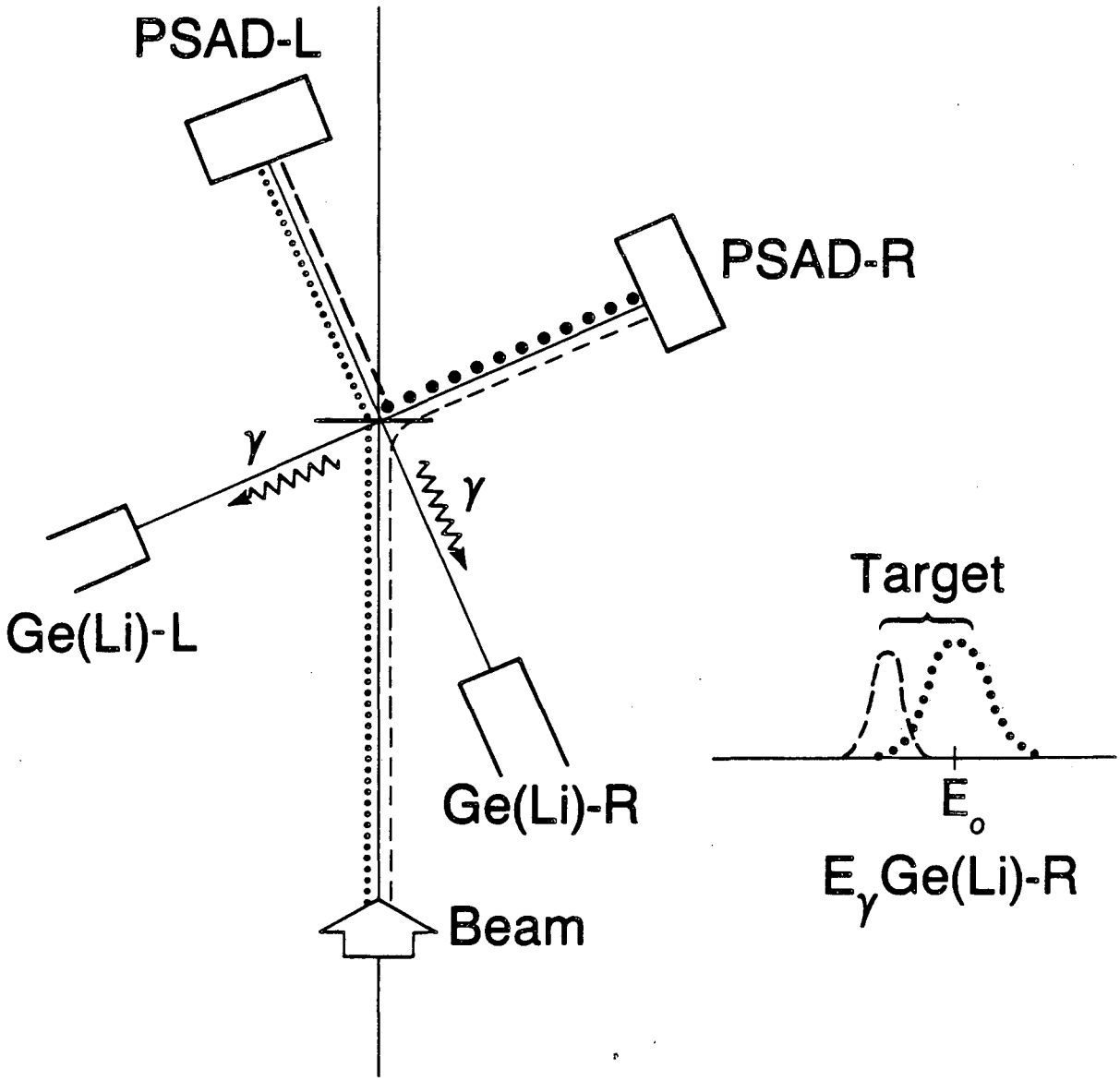

Fig. 1

XBL 841-10005

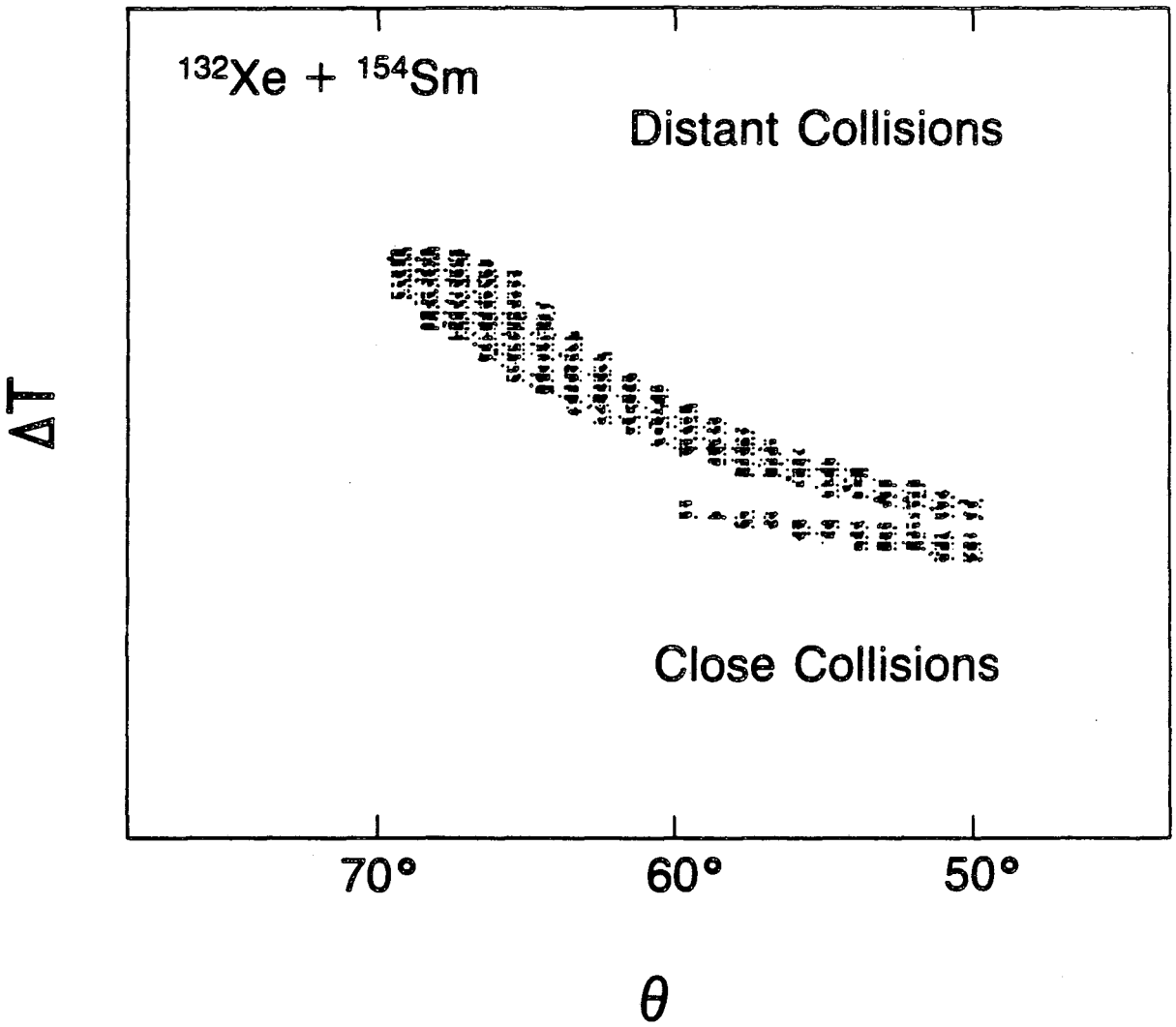

Fig. 2

XBL 841-10010

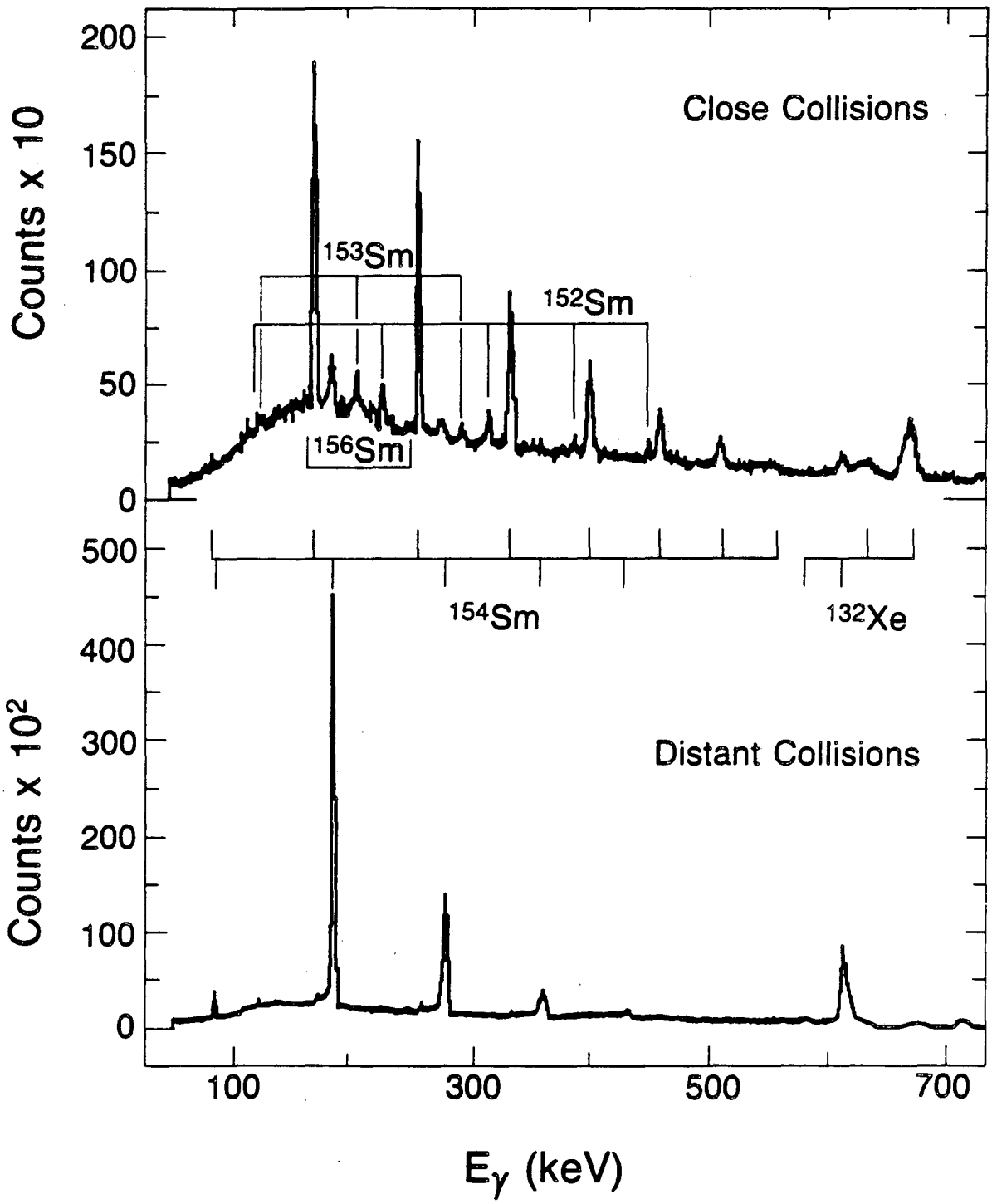

Fig. 3

XBL 843-10127

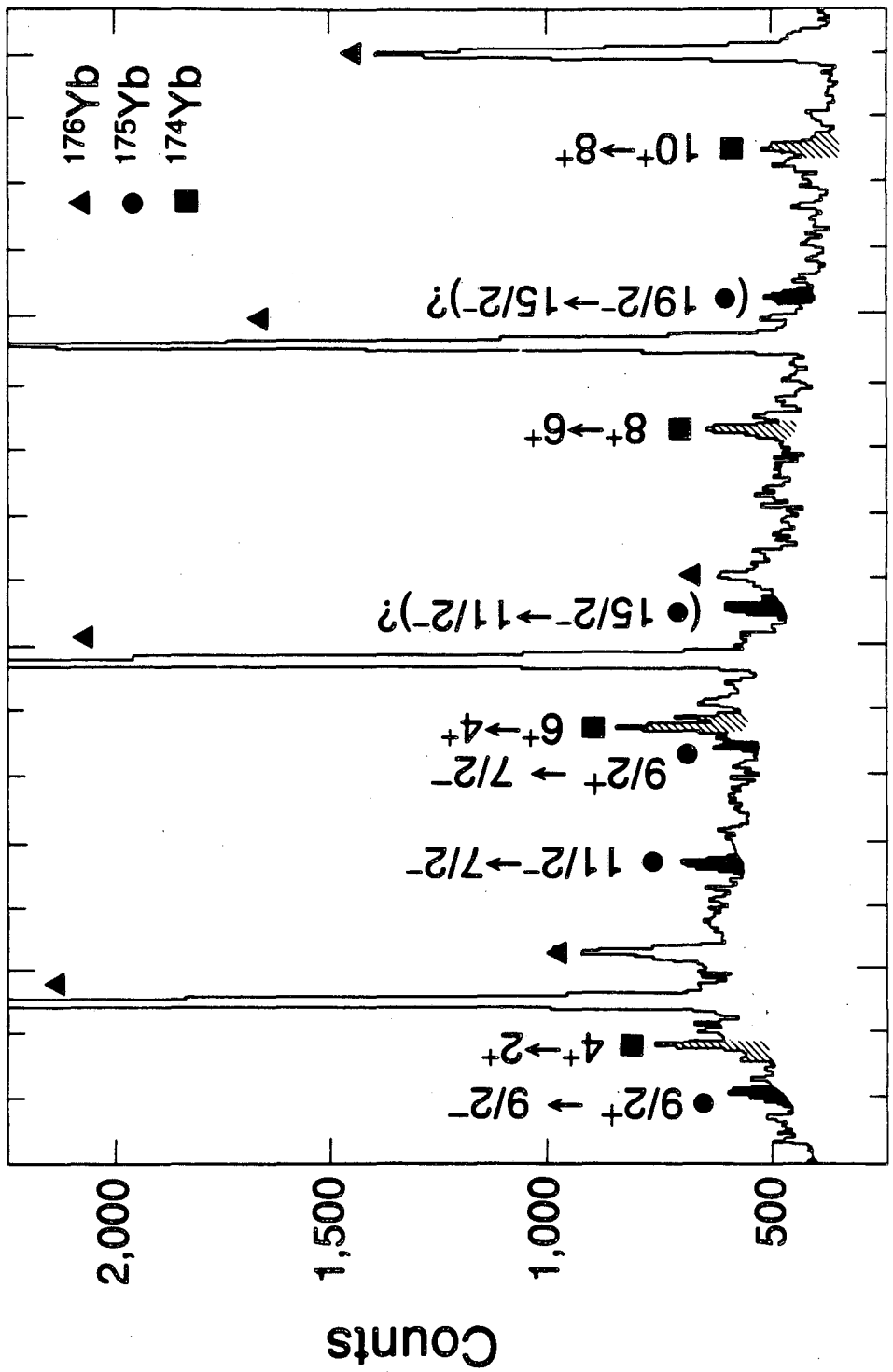

XBL 841-10007

Fig. 4

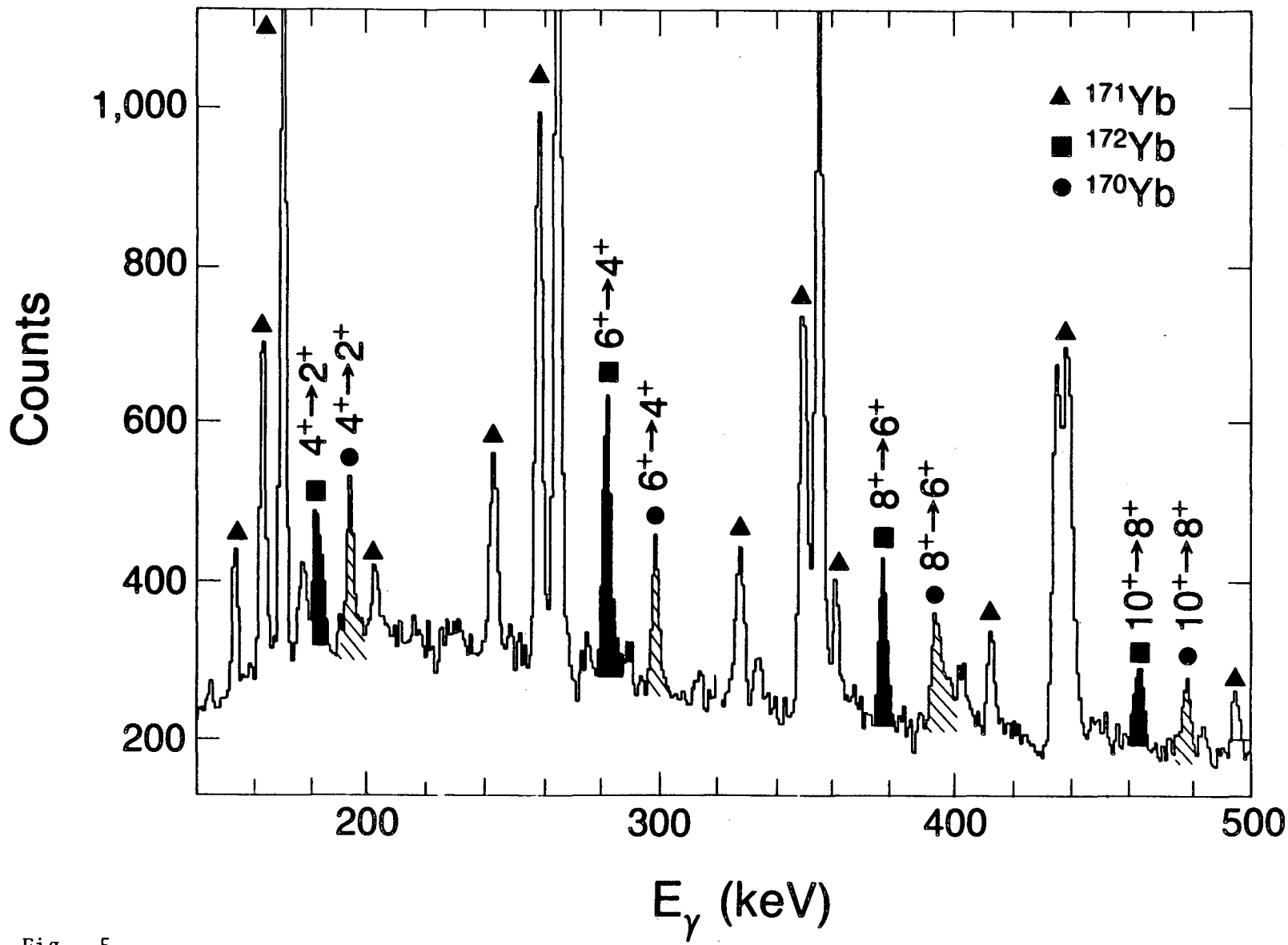

Fig. 5

XBL 841-10014

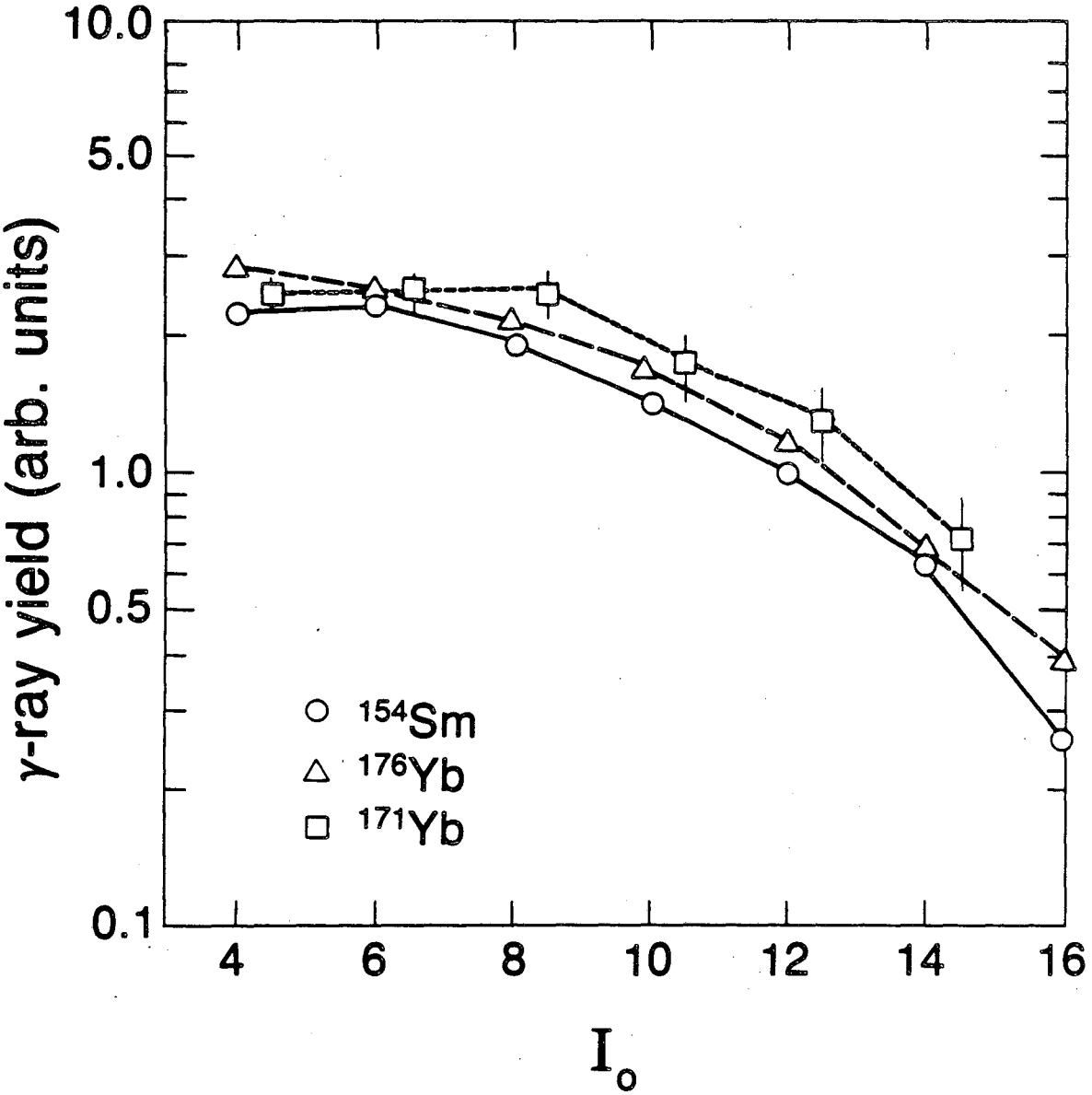

Fig. 6

XBL 841-10008

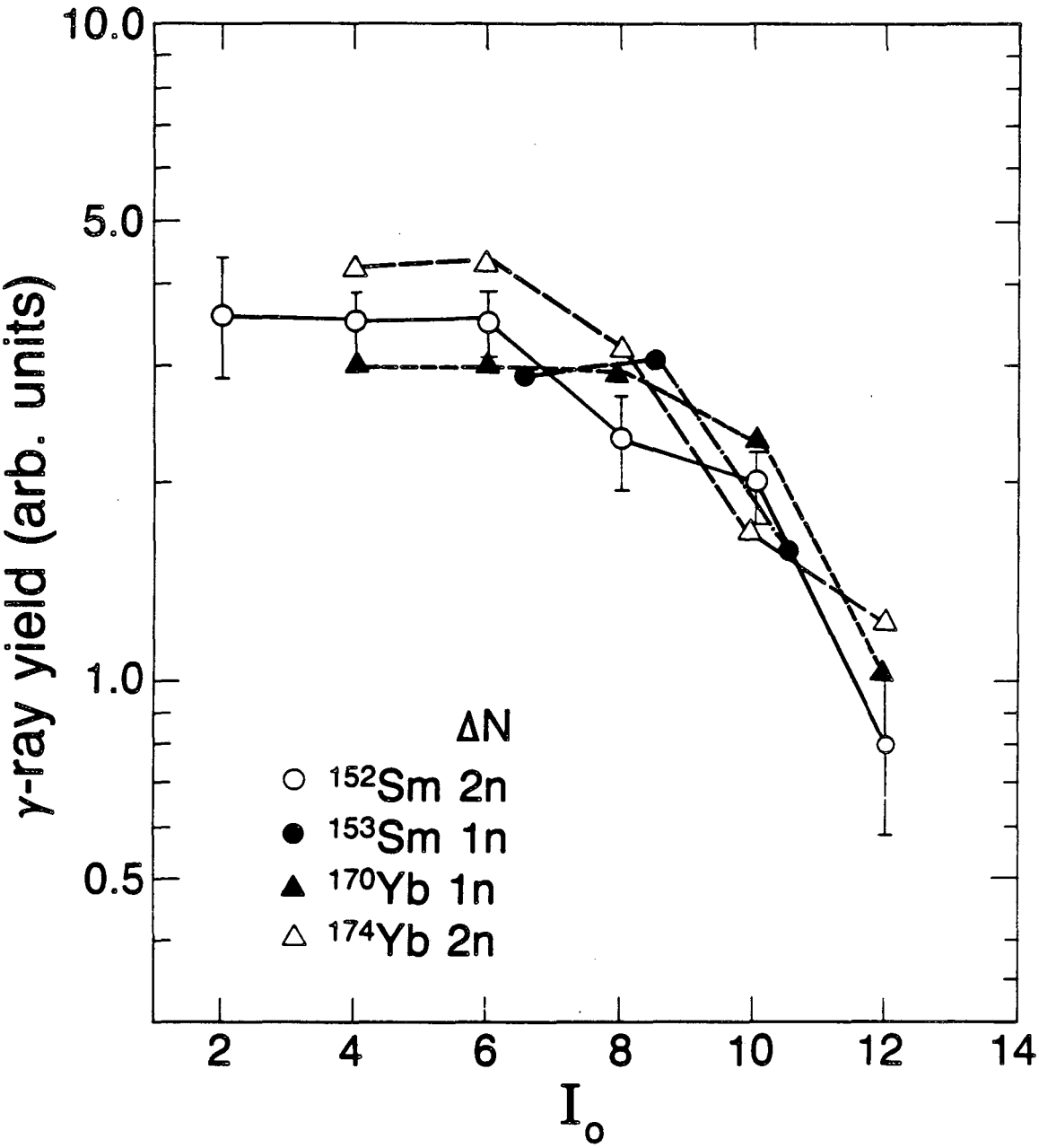

Fig. 7

XBL 841-10012

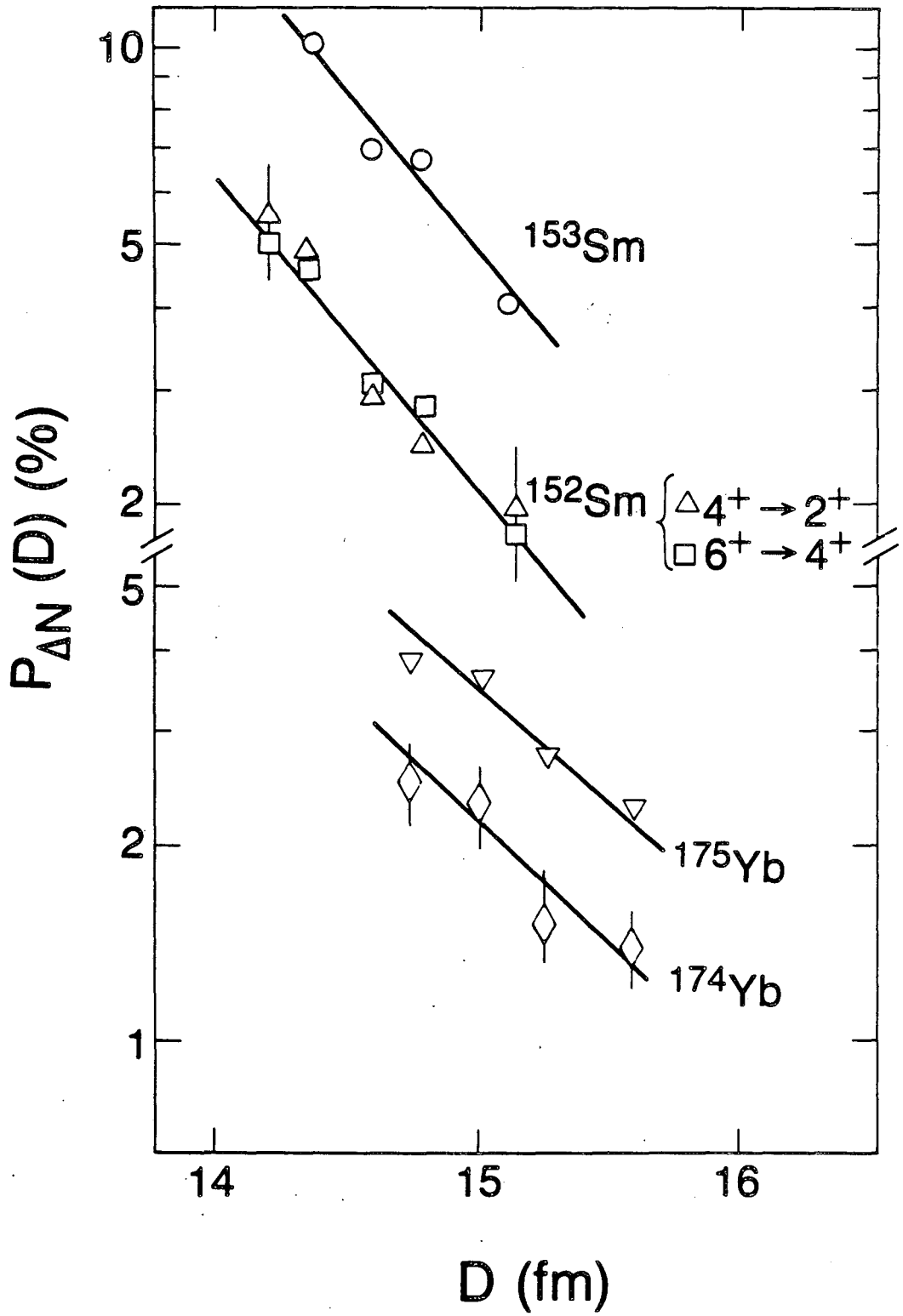

Fig. 8

XBL 843-10125

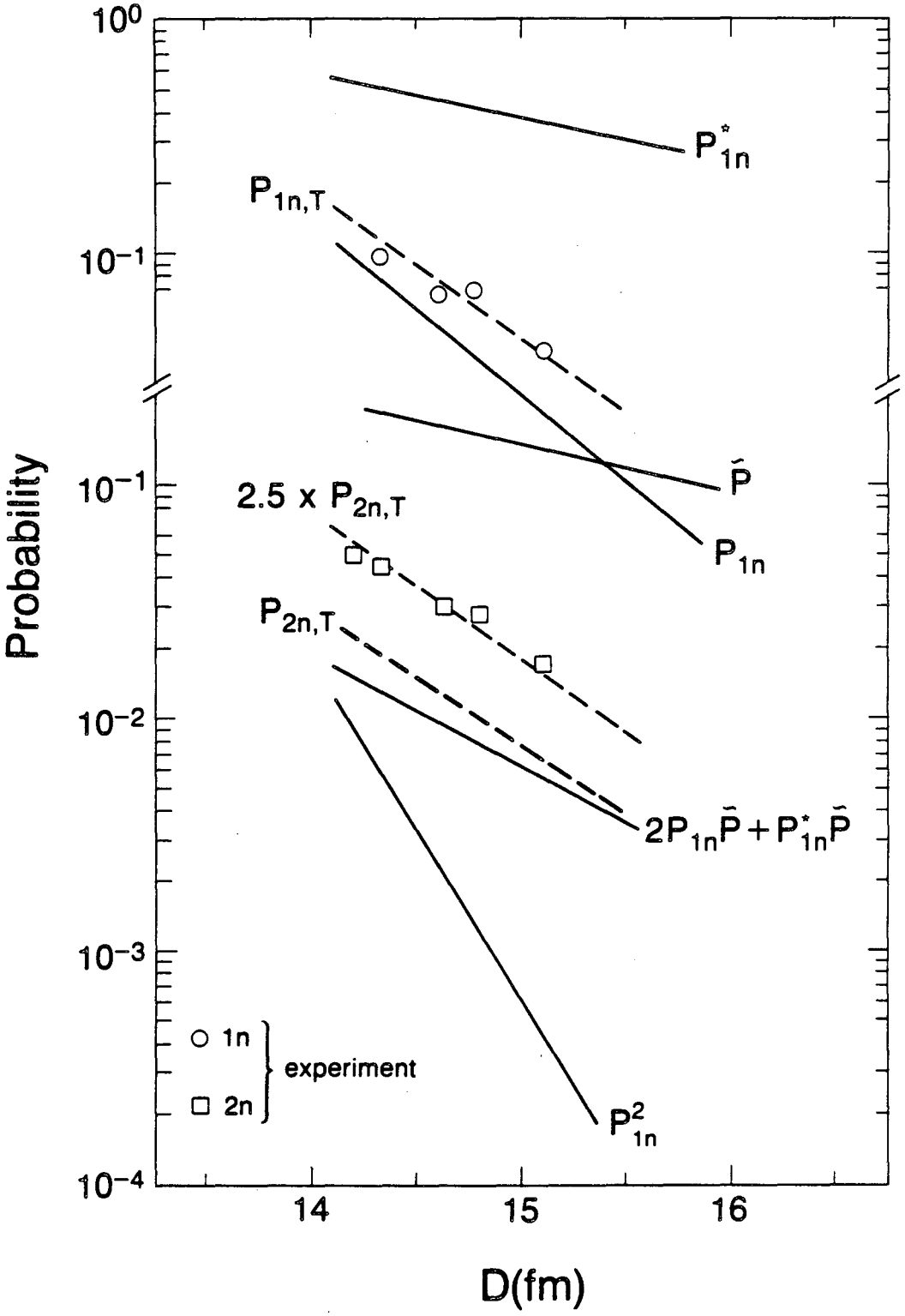

Fig. 9

XBL 843-10126

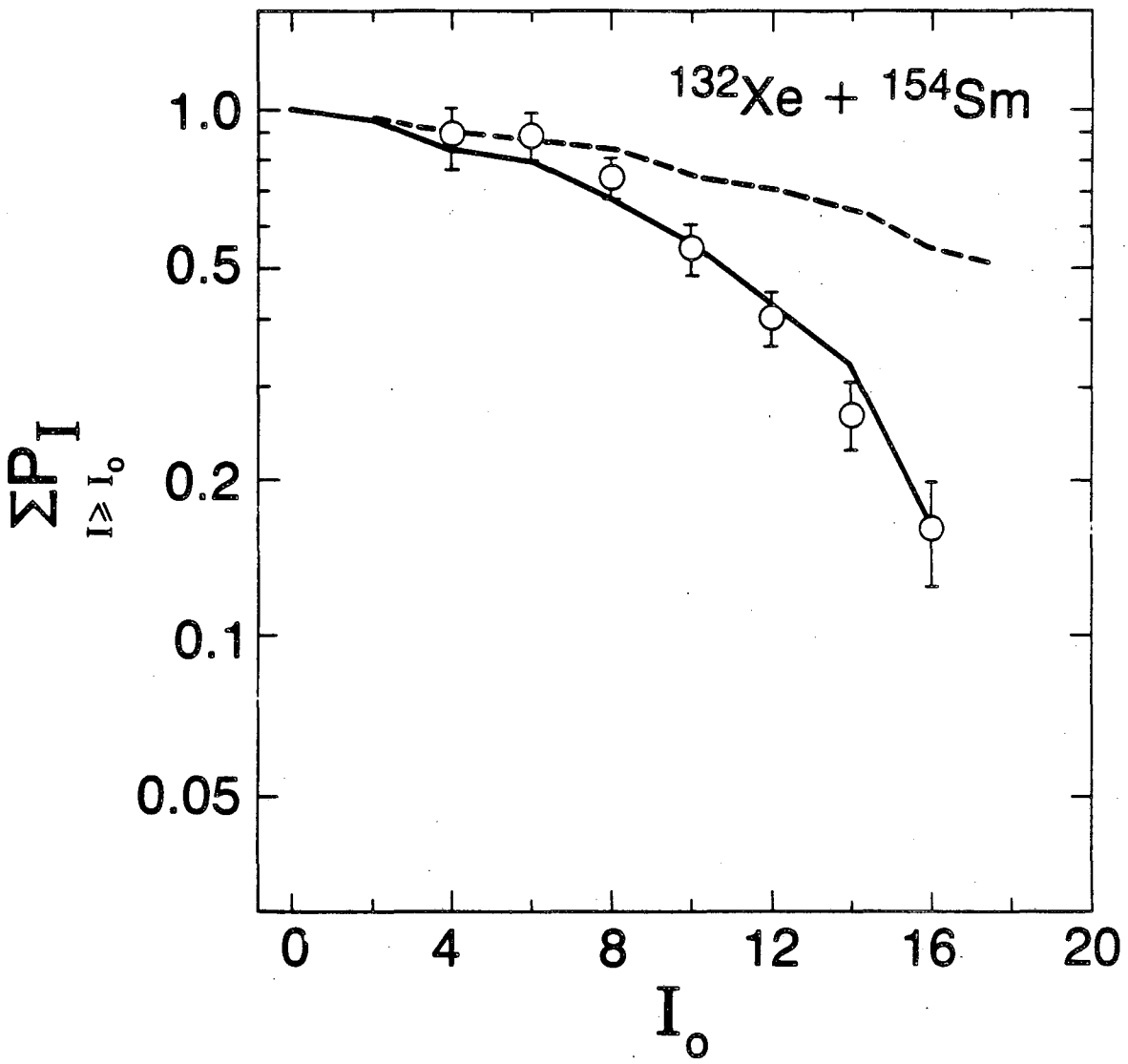

Fig. 10

XBL 841-10006

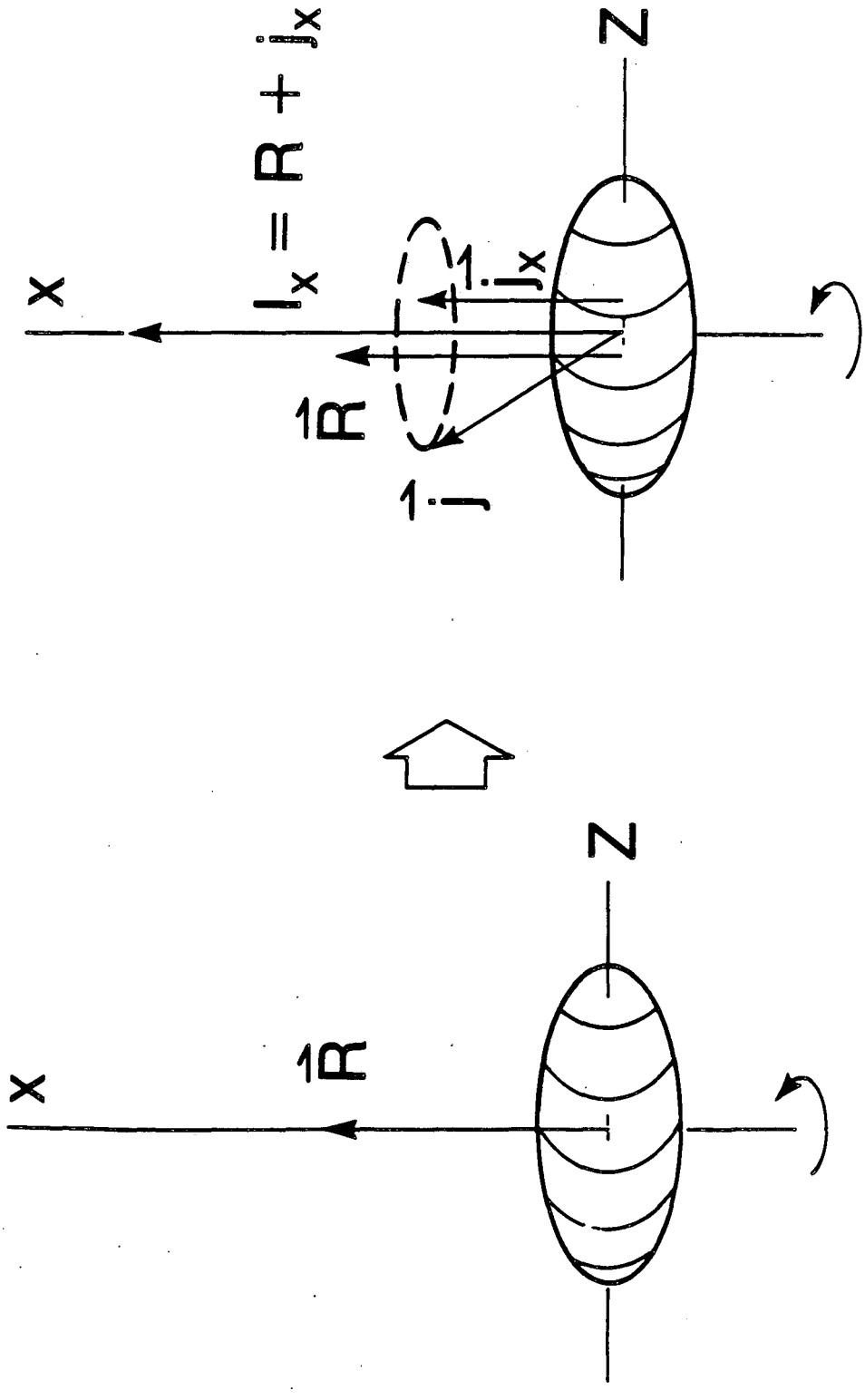

Fig. 11

TECHNICAL INFORMATION DEPARTMENT
LAWRENCE BERKELEY LABORATORY
UNIVERSITY OF CALIFORNIA
BERKELEY, CALIFORNIA 94720